S. Ruoff, M. Stöhr, B. Rauch, G. Eckel, P. Le Clercq, W. Meier, M. Aigner, Numerical simulation and uncertainty quantification of a generic droplet evaporation validation test case, Atomization and Sprays, vol. 30, no. 12, pp. 861-879, 2020

The original publication is available at www.begellhouse.com/

http://dx.doi.org/10.1615/AtomizSpr.2020035295

Atomization and Sprays, x(x):1–23 (2020)

NUMERICAL SIMULATION AND UNCERTAINTY QUANTIFICATION OF A GENERIC DROPLET EVAPORATION VALIDATION TEST CASE

Stephan Ruoff,* Michael Stöhr, Bastian Rauch, Georg Eckel, Patrick Le Clercq, Wolfgang Meier, & Manfred Aigner

German Aerospace Center (DLR), Institute of Combustion Technology, Stuttgart, Germany

*Address all correspondence to: Stephan Ruoff, E-mail: stephan.ruoff@dlr.de

Original Manuscript Submitted: mm/dd/yyyy; Final Draft Received: mm/dd/yyyy

Alternative jet fuels have a high potential to reduce emissions in aviation. A big difficulty for their introduction is the costly and lengthy assessment of fuel effects on combustion performance. In the present work, the evaporation of free-falling droplets of realistic size ($D \approx 80\,\mu\mathrm{m}$) in a well-defined vertical laminar heated flow is studied experimentally and numerically. Measurements of droplet diameters and velocities using microscopic double-pulse shadowgraphy are conducted for several single species and systematically chosen conventional and alternative multi-component jet fuels. The results show that the experiment is fuel-sensitive with respect to evaporation. In this study, special attention is paid to unknown or uncertain boundary and initial conditions, which serve as input in the validation of the numerical models. Therefore, non-intrusive non-deterministic simulations using Polynomial Chaos Expansion are performed to account for these uncertainties. The uncertainty quantification displays that overall uncertainties are small enough to distinguish between the different fuels and to predict fuel-dependent effects on evaporation. Nevertheless, the uncertainties are not negligible. A sensitivity analysis shows a high sensitivity of the evaporation to the offset of the droplet from the centerline and to the uncertainty of the inflow gas temperature. Reducing the uncertainties of the two above-mentioned conditions is most promising in enhancing the validation experiment.

KEY WORDS: *Uncertainty quantification, Sensitivity analysis, Alternative jet fuels, Multi-component evaporation modeling, Fuel sensitivity*

1. INTRODUCTION

In order to reduce CO_2 emissions of the aviation sector, an increasing percentage of alternative, synthetic components are added to conventional fossil jet fuels (Blakey et al., 2011; Kaltschmitt and Neuling, 2017). Safety regulations therefore require a thorough screening and analysis of these added components and their effect on the engine performance, as done in the research programmes JETSCREEN (2020) and NJFCP (Colket et al., 2017).

Besides chemical properties influencing the chemical reactions, the physical properties that govern atomization and evaporation play an important role for the combustor operability. Recent findings show that preferential vaporization impacts the lean blow-out (LBO) limits (Won et al., 2019) and the emissions (Eckel et al., 2019) of jet-fuel combustors.

Due to the crucial role of evaporation in spray combustion, the development of models for multi-component evaporation is an active research topic. The models can be divided into continuous thermodynamic models (Cooney and Singer, 2019; Hallett, 2000; Le Clercq et al., 2009), distillation curve methods (Burger et al., 2003), discrete-component methods (Ebrahimian and Habchi, 2011; Govindaraju and Ihme, 2016; Lupo and Duwig, 2018; Ra and Reitz, 2009; Tonini and Cossali, 2019) and quasi-discrete models (Sazhin et al., 2011). However, the multi-component evaporation models oftentimes lack a proper validation. This is on the one hand because of unknown fuel compositions in the experiments (Brandt et al., 1998; Sanjosé et al., 2008) or intrusive measurement setups, e.g. using suspension fibers (Chauveau et al., 2008). On the other hand, the experimental data are often limited to single species (Deprédurand et al., 2010; Gounder et al., 2012; Verdier et al., 2017) or a small number of fuel components (Birouk and Gökalp, 2002; Daıf et al., 1998; Maqua et al., 2008; Rauch et al., 2012; Stengele et al., 1999) as well as to boundary conditions, which are far from realistic engine-conditions (Brenn et al., 2007; Wilms, 2005). Unquestionably, all these validation data sets provide valuable information but they do not cover the entire range of application of multi-component evaporation models.

Furthermore, model validation is usually carried out after the validation experiment was designed and data are published. This can lead to situations in which results are very sensitive to certain boundary conditions, which were either not measured at all or not determined with the needed accuracy. The unknown parameters need to be calibrated and in consequence the validation is weak. Although the models used in the simulations must be validated before being used for prediction (Oberkampf and Roy, 2010), they can play a major role in reducing design iterations and improving existing experiments. In this context, a close collaboration and combination of numerical simulation and experiment is desirable. Propagating uncertainties stemming from the experiment through the numerical simulation can help to estimate the effect on the quantities of interest. Consequently, sensitivity studies can be used to identify

the most influential input uncertainties that can then be reduced by optimizing the experiment. Despite the potential benefits of uncertainty analysis in combustion simulations, there are only a few studies found in the literature, e.g. for chemical kinetics (Prager et al., 2013), fuel evaporation (Errante et al., 2018; Lupo and Duwig, 2020; Rauch et al., 2016; Shashank et al., 2011), spray boundary conditions (Van Dam and Rutland, 2016) and spray combustion (Enderle et al., 2020).

Yet, to the authors' knowledge, there is no study available aiming at using the synergy of experiments and non-deterministic numerical simulations to improve both the experiment and the modeling. Therefore, the current study aims to provide accurate validation data for evaporation of single droplets alongside non-deterministic simulations propagating input uncertainties that arise from unknown boundary conditions. In contrast to deterministic approaches, a non-deterministic approach eliminates the need to calibrate the uncertain boundary conditions and provides a quantitative measure on the often larger-than-expected uncertainties. Analysis of the propagated uncertainties and sensitivities allow a methodological improvement of the experimental setup and thus minimize the uncertainties.

The paper is structured as follows. An experiment where droplets of realistic size ($D \approx 80\,\mu\mathrm{m}$) are injected in a laminar pre-heated flow is presented in section 2. Next, a summary of the numerical modeling (section 3) and the investigated four single-component and four multi-component fuels (section 4) is given. Measurement results of droplet diameters over time are provided in section 5. Thereafter, the methods used for uncertainty quantification are described (section 6), followed by the results of the non-intrusive non-deterministic simulations of the droplet's evaporation behavior (section 7). Finally, the findings are discussed and conclusions are drawn in section 8.

2. EXPERIMENTAL SETUP

The fuel droplet evaporation is measured in a vertical channel sketched in Fig. 1(a). An air flow of $30\,\mathrm{g/min}$ is electrically heated to $T \approx 250\,^{\circ}\mathrm{C}$, passes through a porous bronze matrix and then flows downwards with an average velocity of about $0.2\,\mathrm{m/s}$ in a channel of $60 \times 60\,\mathrm{mm}^2$ cross-section. Optical access for shadowgraphy is provided by utilizing quartz glass for the channel side walls. A piezo-driven dispenser head (Microdrop MD-K-140) is located above the bronze matrix and injects single droplets of $D \approx 80\,\mu\mathrm{m}$ into a vertical steel tube whose exit is located $5\,\mathrm{mm}$ below the matrix. The droplets are generated periodically with a frequency of $40\,\mathrm{Hz}$, which ensures that the distance between droplets is larger than 200 diameters and thus prevents inter-droplet interaction. An air flow of $0.5\,\mathrm{g/min}$ and $T \approx 30\,^{\circ}\mathrm{C}$ is generated in the vertical tube below the droplet generator resulting in a fully developed laminar flow with an average velocity of about $1\,\mathrm{m/s}$. The flow conditions equate to a Reynolds number of $\mathrm{Re} \approx 300$ and an average droplet Reynolds number of $\mathrm{Re}_d \approx 0.3$. Therefore, well-defined boundary conditions in terms of

velocity and temperature are available for the droplet evaporation domain. The evolution of droplet diameter and velocity is measured using microscopic double-pulse shadowgraphy. The laser pulses from a dual-cavity Nd:YAG-Laser ($\lambda = 532\,\mathrm{nm}$, $E = 2 \times 80\,\mathrm{mJ}$, $50 \leq \Delta t \leq 200\,\mu\mathrm{s}$) are widened by a concave lens and then directed onto a fluorescent screen of $d = 100\,\mathrm{mm}$, which provides the required non-coherent illumination. Resulting double-images of the droplet shadow are recorded using a long-distance microscope (Questar QM100) mounted on a CCD camera ($1.4\,\mathrm{MP}$). The droplet size $D(z)$ and axial velocity $v(z)$ are calculated from the image pairs by an in-house image processing code. For the variation of z, the channel is moved vertically using a translation stage while the optical setup remains fixed. Thereby, measurements of $D(z)$ and $v(z)$ are made every $\Delta z = 5\,\mathrm{mm}$ starting from $z_0 = 1\,\mathrm{mm}$ until the droplet is fully vaporized. The corresponding times $t(z)$ are calculated using the measured velocities as $t(z) = \int_{z_0}^{z} 1/v\,\mathrm{d}z$.

It is noteworthy that the experiment can also be operated with a matrix burner instead of the electrical heater, which enables investigation of droplet evaporation at temperatures up to $1200\,\mathrm{K}$, as demonstrated in a recent study (Stöhr et al., 2020).

3. NUMERICAL MODELING

3.1 Gas flow solver

Simulations are carried out using the DLR in-house CFD code THETA (Di Domenico et al., 2011), which employs a 3D finite-volume solver for unstructured grids. The underlying equations are the conservation of mass, momentum, species and enthalpy. Due to the low flow velocities, buoyancy effects are included in the convection-diffusion equations for heat and species. The convective and diffusive fluxes are discretized using second-order upwind and central schemes, respectively. The Navier-Stokes equations are solved using the Semi-implicit Method for Pressure Linked Equations (SIMPLE).

The computational domain is displayed in Fig. 1(b). It consists of a cylinder at the top and a cuboid representing the droplet tube and the channel, respectively. The fully unstructured grid possesses a strong clustering near the walls and close to the liquid injection system to resolve boundary effects and the droplet evaporation.

3.2 Dispersed phase solver

For the simulation of the liquid phase, THETA is coupled to the DLR in-house solver SPRAYSIM (Eckel et al., 2016), which uses a Lagrangian particle tracking framework. Due to the low frequency of the droplet generator, the mass

and momentum source terms in the gas field equations are negligible. As a consequence, only a one-way coupling is established.

The liquid consists of a multi-component mixture based on the chemical analysis of the individual jet fuels by means of a comprehensive 2D gas chromatography coupled with a mass spectrometry (GCxGC-MS) system. Differences in volatility of the individual species are modeled by two types of multi-component evaporation models. For fuels with a few components, i.e. the four single-component fuels (iso-octane, n-decane- n-dodecane, 1-hexanol) and the B1 fuel (Alcohol-to-Jet), a discrete-component method (DCM) is used. For complex fuels with a large number of components, i.e. A1, C1, and C5 fuels, the continuous thermodynamics model (CTM) of Le Clercq et al. (2009) and Doué et al. (2006) is applied. It assumes that the species distribution can be approximated by a continuous description via probability density functions (Hallett, 2000). The fuel components are grouped into fuel families (n-alkanes, iso-alkanes, cyclo-alkanes, mono-aromatics, di-aromatics), as shown exemplarily in Fig. 2. In the paper at hand, the probability density function (PDF) of each family follows a Γ-distribution. This reduces the number of degrees of freedom in the evaporation model by orders of magnitude, which cuts down the computational costs. The underlying evaporation model for DCM and CTM is the model of Abramzon and Sirignano (1989) with slightly modified terms for Reynolds-dependence (Eckel et al., 2018). It assumes rapid mixing within the droplet.

The Biot number is in the order of $\mathrm{Bi} \approx 0.11$ and thus only slightly above the limit for a "thermally thin" medium ($\mathrm{Bi} = 0.1$), justifying the rapid mixing model's assumption of a uniform temperature inside the droplet. With respect to species diffusion in multi-component droplets, the Lewis number shows values in the order of $\mathrm{Le} \approx 37$. Thus, species diffusion is clearly slower than the heat diffusion. However, internal convection can significantly increase the species mass transfer inside the droplet. In this regard, Wilms (2005), who used rainbow refractometry in a setup similar to this study, observed no species gradients inside the droplets during evaporation. He assumed that the droplet generator induced an internal circulation of the liquid, which persists during the evaporation process. The existence of inner circulations supports the assumption of rapid mixing.

3.3 Boundary conditions

The heated matrix is modeled as a source of hot gas with a pre-defined constant mass flow rate and temperature. The lateral boundaries are represented by isothermal walls. A fixed pressure is applied at the outlet. The experimental setup does not allow a direct measurement of the initial droplet diameter and droplet velocities because the droplet generator is located inside a tube without optical access (Fig. 1 (a)). Therefore, the droplet initial conditions are taken from the manufacturer's specifications listed in Table 2. As previously mentioned, the droplet composition matches

the different fuel compositions determined by chemical analysis (see section 4).

4. FUELS

For the present study two sets of fuels were selected that provide a broad variation of physical properties in order to analyze their effects on the evaporation characteristics. The first group consists of four single-component fuels (iso-octane, n-decane, n-dodecane, 1-hexanol) with different boiling points (Fig. 3). They are used to analyze the quality of the DCM evaporation model. The second group consists of four multi-component fuels that represent a wide range of possible conventional and alternative jet-fuels. They were selected by the JETSCREEN research programme (JETSCREEN, 2020) and are used to explore the limits of the CTM evaporation model in this study. The composition of the multi-component fuels is listed in Table 1.

5. EXPERIMENTAL RESULTS

First, the experimental results of the droplet evaporation for the single component fuels are discussed by means of Fig. 4. The experiments reveals the volatility differences between the fuels. After a short initial heat-up phase, the droplets behave according to the D^2-law, evaporating at constant temperature (Law, 1982). While the three alkanes follow the trend of their respective boiling temperatures T_b, 1-hexanol evaporates slower than n-dodecane despite its lower T_b. This is explained by the higher heat of vaporization of 1-hexanol ($H_v = 603\,\mathrm{J/g}$) in comparison to the one of n-dodecane ($H_v = 361\,\mathrm{J/g}$) (Kim et al., 2019). A more detailed discussion of the (temperature-dependent) influence of latent heat on evaporation rate is provided in our recent study (Stöhr et al., 2020).

Second, Fig. 5 displays the droplet evaporation for the multi-component fuels. After the initial phase of heating and thermal expansion, the evaporation of the lighter fuel components starts. Especially for the B1 fuel the differences between the lighter, fast evaporating and the heavier, slow evaporating components are apparent. The reason for this is that B1 mainly contains two components, iso-dodecane (highly-branched $C_{12}H_{26}$) and iso-cetane (highly-branched $C_{16}H_{34}$). The order of the evaporation of the remaining fuels is in agreement with the distillation curves, where A1 evaporates first, followed by C5 and C1. The differences between the multi-component fuels are measured with high precision.

6. NON-DETERMINISTIC (PROBABILISTIC) APPROACH FOR UNCERTAINTY QUANTIFICATION

Sources of uncertainty can be partitioned into three categories: numerical, model form and input uncertainties (Oberkampf and Roy, 2010). The present study focuses on the impact of input uncertainties on a quantity of interest Q.

Input uncertainties include parameters used in the simulation model and boundary conditions. The input uncertainties are propagated through the simulation model $\mathcal{M}$ by a non-intrusive method, where $\mathcal{M}$ is considered as a black-box and the probabilistic behavior is achieved from a finite number of random samples of $\mathcal{M}$ (Roy and Oberkampf, 2011).

6.1 Uncertainty propagation

The most clear-cut sampling technique is the Monte Carlo method (Fishman, 2013). However, this technique requires a large number of samples to return reliable statistics, making it unsuitable for large scale simulation problems. Therefore, it is replaced by a surrogate model using Polynomial Chaos Expansion (PCE) (Le Maître and Knio, 2010; Xiu and Karniadakis, 2003) on a sparse grid (Smolyak, 1963). A typical PCE of the quantity Q, driven by n inputs $\vec{\xi} = (\xi_1, \ldots, \xi_n)$ is given as

$$Q = f(\xi) \approx \sum_{k=0}^{P} \alpha_k \Psi_k(\vec{\xi}) = \mathcal{M}_{PCE}\,, \tag{1}$$

where α_k are the modes and Ψ_k are multivariate polynomials of $\vec{\xi}$. The approximation of the typically infinite series depends on the total degree p of the multivariate polynomials Ψ_k leading to $P+1 = (n+p)!/(n!p!)$, where P is the truncation order of the series. For a given PCE the mean $\mathbb{E}$ and variance $\mathbb{V}$ are directly calculated as

$$\mathbb{E} = \alpha_0 \quad \text{and} \quad \mathbb{V} = \sum_{k=0}^{P} \alpha_k^2 \langle \Psi_k^2 \rangle\,. \tag{2}$$

6.2 Sensitivity analysis

Subsequent to the uncertainty quantification with PCE, the resulting model approximation $\mathcal{M}_{PCE}$ is used to directly calculate the sensitivities of the quantity of interest Q to the inputs $\vec{\xi}$. The sensitivities are computed by variance-based decomposition of the entire variance $\mathbb{V}$ of the model output $\mathcal{M}(\vec{\xi})$ into contributions of the different inputs $\mathbb{V}[\mathcal{M}(\vec{\xi})|\xi_i]$ (Sobol, 1993; Sudret, 2008). The so-called Sobol indices

$$S_i = \frac{\mathbb{V}\left[\mathbb{E}\left[\mathcal{M}(\vec{\xi})|\xi_i\right]\right]}{\mathbb{V}\left[\mathcal{M}(\vec{\xi})\right]} \quad \text{and} \quad S_i^T = \frac{\mathbb{V}\left[\mathbb{E}\left[\mathcal{M}(\vec{\xi})|\xi_{\sim i}\right]\right]}{\mathbb{V}\left[\mathcal{M}(\vec{\xi})\right]} \tag{3}$$

represent the main effect and the total effect indices, respectively. The main effect indices S_i correspond to the direct contributions of ξ_i to the variance of $\mathcal{M}$, whereas S_i^T also include interactions with other variables.

6.3 Definition of the UQ problem

The aforementioned methods are applied to the numerical simulation of the evaporation test case. Sandia DAKOTA 6.10 (Adams et al., 2009) is used to construct and evaluate the UQ methods, with the THETA-SPRAYSIM framework as a black-box.

In classical, deterministic, numerical simulations the unknown boundary conditions are estimated or calibrated to yield a best estimate for the known data. Furthermore, the uncertainties of the known boundary conditions could be used to tweak the simulation to fit the experimental data. Therefore, the validation of the model is weak. In this study, the unknown boundary conditions of the gas field are estimated, however the uncertainties introduced by the calibration will be considered in the non-deterministic study.

6.3.1 Definition of boundary conditions

As a first step, before conducting the non-deterministic simulations, the boundary conditions of the gas field and droplet initial conditions are classified by the type of method used to determine their values (Table 2). Except for the wall temperatures of the test case, all other boundary and initial conditions are known. The values and uncertainties of the wall temperatures are estimated as follows. The only information available to determine the wall temperatures are the measurements of the centerline temperature by thermocouples. The wall temperatures are estimated using DAKOTA to meet the measured centerline gas temperatures $T_g(z)$. For this purpose, wall temperatures at three different positions ($z = 0, 100, 200\mathrm{mm}$), interpolated by Akima splines (Akima, 1970) were optimized with an adaptive nonlinear least-squares algorithm (NL2SOL, Dennis Jr et al. (1981)) already implemented in DAKOTA. In contrast to deterministic simulations, the estimation of the wall temperatures in this manner reduces the uncertainties stemming from the unknown boundary conditions rather than disregard them. The best parameters for the wall temperatures yield the results in Fig. 6 and reflect the evolution of the measured centerline temperature. The parameters are listed in the value column of Table 2. In particular, the temperature drop due to buoyancy effects at $z \approx 175\,\mathrm{mm}$ is met correctly. In this respect, it is noteworthy that the temperature drop does not influence the evaporation behavior, since all fuels completely evaporate before. The authors would like to emphasize that only the wall temperatures are determined by a calibration while none of the models used in the gas flow or dispersed flow solver are specifically tuned to the test case.

6.3.2 Quantities of Interest

As a second step, the quantities of interest Q have to be defined. For the uncertainty propagation, the evolution of the normalized squared diameter D^2/D_0^2 over time is chosen as Q. As the examination of each point in time of the temporal diameter evolution would be too extensive for the subsequent sensitivity analysis, three global metrics for the evaporation are chosen. The evaporation rate K, the total evaporation time t_t and the unsteady heat-up time

$$t_{us} = t_t - 1/K \tag{4}$$

are illustrated in Fig. 7. The unsteady heat-up time t_{us} is the time at which $D = D_0$. It is extrapolated back from the total evaporation time t_t using a linear evaporation rate K. Despite the dependency of t_{us} on the other two quantities of interest, it is added to get a better picture of the whole evaporation process.

6.3.3 Characterization of input uncertainties

The third step of the definition of the UQ problem contains the characterization of the input uncertainties. For the sake of clarity, the input uncertainties are divided into two groups, i.e. uncertainties in the flow boundary conditions and uncertainties in the droplet initial conditions. All input quantities are treated as epistemic interval-valued uncertainties, defined by the respective minimum and maximum as summarized in Table 2.

Although the flow boundary conditions have been estimated to meet the measured centerline temperature, they are not free of errors. The thermocouple measurements are subject to measurement errors and are very sensitive to the radial position of the thermocouple. Especially for regions near the tube exit, small deviations in the radius lead to big shifts in the measured temperature. Therefore, an uncertainty of $\pm 15\,\mathrm{K}$ was estimated for the channel wall temperatures T_z at $z = 0$, 100 and 200 mm, with the ambient air temperature as the lower limit. For the wall temperature of the tube T_t as well as the temperature of the heated air inflow T_in, the uncertainties are considered to be $\pm 5\,\mathrm{K}$.

The droplet initial conditions are based on the manufacturer's specifications for the droplet initial diameter D_d and the initial velocity v_d. The uncertainties for the droplet initial conditions are estimated from previous measurements. The droplet temperature T_d is expected to be around the ambient air temperature measured by a thermocouple. Additionally, the uncertainty in the starting position needs to be considered in the UQ study. As can be seen from Fig. 8 showing the droplets' offset r from the centerline, the different single component droplets have slightly different trajectories. This leads to different gas velocities and temperatures seen by the droplet. The uncertainty in the radial position is assumed to be $1.8\,\mathrm{mm}$, which is the maximum offset for n-dodecane at the tube exit ($z = 1\,\mathrm{mm}$).

7. RESULTS OF NON-DETERMINISTIC SIMULATIONS

The PCE surrogate model $\mathcal{M}_{PCE}$ is built by calculating 199 samples defined by the Smolyak quadrature for the $n = 9$ inputs. Hermite orthogonal basis polynomials are used as multivariate polynomials Ψ_k. The accuracy of the surrogate model $\mathcal{M}_{PCE}$ is examined through holdout validation against 20 additional holdout datasets. The normalized root mean squared error is below $1\,\%$ at all vertical positions.

7.1 Results of uncertainty propagation

Initially, the normalized squared diameter evolutions of the single component fuels are compared to the measurement results. Fig. 9 illustrates that the mean $\mathbb{E}$ of the simulations predicts the measured evaporation behavior for all single components. Assessing the uncertainties, the results can be divided into two sections. In the early stages of evaporation, the uncertainties are too large to distinguish between the different fuels. Later, when the droplets behave according to the D^2-law, the difference in evaporation between the three alkanes can be distinguished, i.e. the predicted intervals do not overlap. Not only is the calculated mean in close agreement with the experimental data, but the predicted uncertainties also fully enclose all measurements. Thus, no error is identifiable and the evaporation model is proven to be accurate for the single component fuels. It is also noteworthy that an earlier onset of evaporation inside the tube and a faster evaporation cause the larger uncertainties for iso-octane.

The four multi-component fuels are shown in Fig. 10. For the initial phase $(t/D^2 < 5\,\mathrm{s/mm^2})$, the mean of the simulations match the experimental data for all four fuels. The trend between all four fuels is also predicted correctly. Even though the predicted intervals overlap in the early stages of evaporation, the different fuels can be distinguished in the later stages. Moreover, the fuels A1 and B1 lie within the predicted intervals for the major part of the evaporation process. The deviation of the B1 fuel for later stages of evaporation can be attributed to impurities in the fuel. If the impurity is caused by a heavier fuel component, even an amount $1\,\mathrm{vol}\%$ corresponds to a remaining diameter of $D = 17.2\,\mu\mathrm{m}$ or $D/D_0 = 0.046$, matching the measured values for the later stages of the evaporation. The close agreement of the B1 fuel with the experiments also confirms the assumption of rapid mixing inside the droplet. In contrast to the A1 and B1 fuel, the predicted intervals for C1 and C5 do not cover the measurement data in the later stages of the evaporation.

The discrepancy between the simulation and measurement of the C1 and C5 fuel cannot be accredited to the input uncertainties, which were taken into account in the non-deterministic simulation. As previously shown, the evaporation model is accurate for single-component fuels. Furthermore, the errors associated with use of Γ-functions that don't precisely match the measured compositions were found to be small in a previous study (Ruoff et al., 2019).

Therefore, the deviation has to originate from the CTM evaporation model or the underlying property model. A first analysis suggests that the physical properties predicted by the CTM, e.g. heat capacity (c_p) and heat of vaporization (H_v), of the C-fuels need to be improved. This is presumably related to the high content of di-aromatics in these fuels. A detailed analysis of the CTM property correlations is necessary, which lies outside the scope of this study and will be subject of future work.

7.2 Results of sensitivity analysis

To evaluate the contribution of the uncertain input parameters to the variances in the simulation results, the Sobol indices introduced in Equation 3 are calculated for the A1 reference fuel. The A1 reference fuel is chosen since the prediction for the A1 fuel showed the closest agreement with experimental results. The bars in Fig. 11 illustrate the direct contribution of each input parameter to the variance in each quantity of interest. The total Sobol indices S_i^T and main Sobol indices S_i are nearly identical, indicating very small interactions between the inputs, and are therefore not shown in Fig. 11.

For the evaporation rate K, the inlet temperature of the heated air inflow is identified as the dominant parameter, followed by the radial offset r_d and the tube wall temperature T_t. All of the three parameters influence the ambient temperature, which the droplet experiences along the trajectory. Consequently, the evaporation rate changes.

Likewise, the total evaporation time t_t also depends on parameters influencing the ambient temperature. However, the offset r_d from the centerline has a larger influence. As the gas velocity decreases towards the tube walls due to boundary layer effects, droplets experience longer residence times in the hot regions. Furthermore, the droplet initial diameter D_d contributes directly to t_t since more mass needs to evaporate.

For the unsteady heat-up time t_{us}, the Sobol indices shift towards the droplet initial conditions. Similarly to the total evaporation time, the deviation from the centerline r_d influences the residence time and thus the droplet heat up before entering the channel. Furthermore, a larger initial diameter D_d increases the droplet mass so that more energy is needed to heat up the droplet. Despite of the dependence of t_{us} on t_t and K (Equation 4), the means $\mathbb{E}$ and thus the Sobol indices do not follow the simple relationship because of Jensen's inequality (Jensen et al., 1906): $\xi = K$ is a random variable and $f(\xi) = \frac{1}{\xi}$ is a convex function, thus $f(\mathbb{E}(\xi)) \leq \mathbb{E}(f(\xi))$.

From the previous observations, the flow field parameter causing the largest variance is the matrix inflow temperature T_{in}, whereas the most dominant droplet initial condition is the deviation from the centerline r_d. Together, they account for more than $50\,\%$ of variance in all quantities of interests. Therefore, a reduction of the uncertainty of the matrix inflow temperature T_{in} and a reduction of the offset from the centerline r_d promise to have the biggest impact to

improve the precision of the experiment.

The sensitivity analysis was also performed for the B1 fuel, since it may be sensitive to different input variables. However, the results are very similar, with only slight shifts from r_d to T_{in} for K and t_t. This shift can be explained by the faster evaporation of B1 and thus the evaporation happening closer to the matrix heater.

8. CONCLUSIONS

In the present work, the evaporation of multi-component jet fuels was successfully studied using a combination of experiments and numerical simulations with a detailed uncertainty quantification. The evaporation test case for multi-component fuel droplets of realistic size provides precise measurements of droplet diameters over time. For all tested fuels, the composition is well characterized and the difference of their evaporation behavior is measured with high precision. The measurements of conventional and alternative jet fuels also capture the different stages of multi-component evaporation behavior, such as droplet heating, fast evaporation of light components and slow evaporation of heavy components.

Based on the results and boundary conditions of the measurements, the evaporation model was validated by means of non-deterministic numerical simulations. The input uncertainties, introduced from boundary and initial conditions of the experiment, were propagated through the model by non-intrusive non-deterministic simulations. Furthermore, uncertainties associated with the estimation of the unknown boundary conditions were propagated. The uncertainty quantification revealed that for all fuels modeled with the DCM the experimental data is within the probabilistic bounds. In contrast, for two of the three multi-component fuels the measurement data were outside the predicted intervals after 65 $\mathrm{vol}\,\%$ had evaporated. As input uncertainties are propagated through the simulation, the deviation has to be attributed to an error in the CTM evaporation or property model. This error shows that an examination of the CTM evaporation model uncertainties is necessary, but is beyond the scope of the present study. Additionally, the close agreement of the binary B1 fuel mixture's calculations with the experiment confirms the assumption of rapid mixing inside the droplet. The sensitivity analysis reveals that the majority of variance in all quantities of interest is related to the uncertainties in the matrix inlet temperature and the offset of the droplets from the centerline.

To conclude, the test case provides suitable validation data for aviation-relevant fuels. However, the UQ shows that the uncertainties from uncharacterized boundary conditions are not negligible. From the findings of the sensitivity analysis, the authors propose that the most promising enhancement for the validation experiment would be a reduction of uncertainties in the matrix inlet temperature and in the reduction of the offset of the droplets from the centerline. Finally, both the experiment and simulation profit from a close collaboration, as the non-deterministic approach gives

insight to sources of errors and provides quantitative data for the methodological improvement of the validation experiment.

ACKNOWLEDGMENTS

DLR has received funding from the European Union's Horizon 2020 research and innovation programme under grant agreement No. 723525. The authors gratefully acknowledge the Gauss Centre for Supercomputing e.V. (www.gauss-centre.eu) for funding this project by providing computing time on the GCS Supercomputer SuperMUC-NG at Leibniz Supercomputing Centre (www.lrz.de). Additionally, the authors want to thank Dr. Patrizio Massoli for the in-depth discussion about the non-deterministic nature of experimental results and the importance to take these into account for reliable numerical simulations.

REFERENCES

Abramzon, B. and Sirignano, W., Droplet vaporization model for spray combustion calculations, *International journal of heat and mass transfer*, vol. **32**, no. 9, pp. 1605–1618, 1989.

Adams, B.M., Bohnhoff, W., Dalbey, K., Eddy, J., Eldred, M., Gay, D., Haskell, K., Hough, P.D., and Swiler, L.P., Dakota, a multilevel parallel object-oriented framework for design optimization, parameter estimation, uncertainty quantification, and sensitivity analysis: version 5.0 user's manual, *Sandia National Laboratories, Tech. Rep. SAND2010-2183*, 2009.

Akima, H., A new method of interpolation and smooth curve fitting based on local procedures, *Journal of the ACM (JACM)*, vol. **17**, no. 4, pp. 589–602, 1970.

Asrardel, M., Muelas, A., and Ballester, J., Assessment of Uncertainties in Predicted Evaporation Rates of Diesel Droplets, 2019, poster presented at the 11th Mediterranean Symposium, Tenerife, Spain.

ASTM International, ASTM D86, Standard Test Method for Distillation of Petroleum Products at Atmospheric Pressure, 2004.

Birouk, M. and Gökalp, I., A new correlation for turbulent mass transfer from liquid droplets, *International Journal of Heat and Mass Transfer*, vol. **45**, no. 1, pp. 37–45, 2002.

Blakey, S., Rye, L., and Wilson, C.W., Aviation gas turbine alternative fuels: A review, *Proceedings of the combustion institute*, vol. **33**, no. 2, pp. 2863–2885, 2011.

Brandt, M., Rachner, M., and Schmitz, G., An experimental and numerical study of kerosine spray evaporation in a premix duct for gas turbine combustors at high pressure, *Combustion Science and Technology*, vol. **138**, no. 4, pp. 313 – 348, 1998.

Brenn, G., Deviprasath, L., Durst, F., and Fink, C., Evaporation of acoustically levitated multi-component liquid droplets, *International Journal of Heat and Mass Transfer*, vol. **50**, no. 25, pp. 5073 – 5086, 2007.

Burger, M., Schmehl, R., Prommersberger, K., Schäfer, O., Koch, R., and Wittig, S., Droplet evaporation modeling by the distillation curve model: accounting for kerosene fuel and elevated pressures, *International journal of heat and mass transfer*, vol. **46**, no. 23, pp. 4403–4412, 2003.

Chauveau, C., Halter, F., Lalonde, A., and Gökalp, I., An experimental study on the droplet vaporization: effects of heat conduction through the support fiber, *22nd Annual Conference on Liquid Atomization and Spray Systems (ILASS-Europe 2008)*, Como, Italy, 2008.

Colket, M., Heyne, J., Rumizen, M., Gupta, M., Edwards, T., Roquemore, W.M., Andac, G., Boehm, R., Lovett, J., Williams, R., , Overview of the national jet fuels combustion program, *AIAA Journal*, pp. 1087–1104, 2017.

Cooney, A.Y. and Singer, S.L., A hybrid droplet vaporization-chemical surrogate approach for emulating vaporization, physical properties, and chemical combustion behavior of multicomponent fuels, *Proceedings of the Combustion Institute*, vol. **37**, no. 3, pp. 3229 – 3236, 2019.

Daıf, A., Bouaziz, M., Chesneau, X., and Cherif, A.A., Comparison of multicomponent fuel droplet vaporization experiments in forced convection with the sirignano model, *Experimental Thermal and Fluid Science*, vol. **18**, no. 4, pp. 282–290, 1998.

Dennis Jr, J.E., Gay, D.M., and Welsch, R.E., Algorithm 573: Nl2sol—an adaptive nonlinear least-squares algorithm [e4], *ACM Transactions on Mathematical Software (TOMS)*, vol. **7**, no. 3, pp. 369–383, 1981.

Deprédurand, V., Castanet, G., and Lemoine, F., Heat and mass transfer in evaporating droplets in interaction: Influence of the fuel, *International Journal of Heat and Mass Transfer*, vol. **53**, no. 17, pp. 3495 – 3502, 2010.

Di Domenico, M., Gerlinger, P., and Noll, B., Numerical simulations of confined, turbulent, lean, premixed flames using a detailed chemistry combustion model, *ASME 2011 Turbo Expo: Turbine Technical Conference and Exposition*, ASME Digital Collection, pp. 519–530, 2011.

Doué, N., Le Clercq, P., and Aigner, M., Validation of a multicomponent-fuel droplet evaporation model based on continuous thermodynamics, *International Congress on Liquid Atomization and Spray Systems*, 2006.

Ebrahimian, V. and Habchi, C., Towards a predictive evaporation model for multi-component hydrocarbon droplets at all pressure conditions, *International Journal of Heat and Mass Transfer*, vol. **54**, no. 15, pp. 3552 – 3565, 2011.

Eckel, G., Grohmann, J., Cantu, L., Slavinskaya, N., Kathrotia, T., Rachner, M., Clercq, P.L., Meier, W., and Aigner, M., Les of a swirl-stabilized kerosene spray flame with a multi-component vaporization model and detailed chemistry, *Combustion and Flame*, vol. **207**, pp. 134 – 152, 2019.

Eckel, G., Le Clercq, P., Kathrotia, T., Saenger, A., Fleck, S., Mancini, M., Kolb, T., and Aigner, M., Entrained flow gasification. part 3: Insight into the injector near-field by large eddy simulation with detailed chemistry, *Fuel*, vol. **223**, pp. 164–178, 2018.

Eckel, G., Rachner, M., Le Clercq, P., and Aigner, M., Semi-empirical model for the unsteady shear breakup of liquid jets in cross-flow, *Atomization and Sprays*, vol. **26**, no. 7, 2016.

Enderle, B., Rauch, B., Grimm, F., Eckel, G., and Aigner, M., Non-intrusive uncertainty quantification in the simulation of turbulent spray combustion using polynomial chaos expansion: A case study, *Combustion and Flame*, vol. **213**, pp. 26 – 38, 2020.

Errante, P., Corre, C., and Makhlouf, S., Uncertainty quantification for the eulerian-lagrangian simulation of evaporating sprays, *Proceedings of the 14th Triennial International Conference on Liquid Atomization and Spray Systems*, pp. 1–8, 2018.

Fishman, G., *Monte Carlo: concepts, algorithms, and applications*, Springer Science & Business Media, 2013.

Gounder, J.D., Kourmatzis, A., and Masri, A.R., Turbulent piloted dilute spray flames: Flow fields and droplet dynamics, *Combustion and Flame*, vol. **159**, no. 11, pp. 3372 – 3397, 2012.

Govindaraju, P.B. and Ihme, M., Group contribution method for multicomponent evaporation with application to transportation fuels, *International Journal of Heat and Mass Transfer*, vol. **102**, pp. 833–845, 2016.

Hallett, W.L., A simple model for the vaporization of droplets with large numbers of components, *Combustion and Flame*, vol. **121**, no. 1-2, pp. 334–344, 2000.

Jensen, J.L.W.V. , Sur les fonctions convexes et les inégalités entre les valeurs moyennes, *Acta mathematica*, vol. **30**, pp. 175–193, 1906.

JETSCREEN, JET Fuel SCREENing and Optimization, 2020, 06.2017–10.2020, European Union's Horizon 2020 research and innovation programme under grant agreement No 723525. `https://cordis.europa.eu/project/id/723525`

Kaltschmitt, M. and Neuling, U., *Biokerosene: Status and Prospects*, Springer, 2017.

Kim, S., Chen, J., Cheng, T., Gindulyte, A., He, J., He, S., Li, Q., Shoemaker, B.A., Thiessen, P.A., Yu, B., , Pubchem 2019 update: improved access to chemical data, *Nucleic acids research*, vol. **47**, no. D1, pp. D1102–D1109, 2019.

Law, C., Recent advances in droplet vaporization and combustion, *Progress in energy and combustion science*, vol. **8**, no. 3, pp. 171–201, 1982.

Le Clercq, P., Doué, N., Rachner, M., and Aigner, M., Validation of a multicomponent-fuel model for spray computations, *47th AIAA Aerospace Sciences Meeting including The New Horizons Forum and Aerospace Exposition*, p. 1188, 2009.

Le Maître, O. and Knio, O.M., *Spectral methods for uncertainty quantification: with applications to computational fluid dynamics*, Springer Science & Business Media, 2010.

Lupo, G. and Duwig, C., A numerical study of ethanol–water droplet evaporation, *Journal of Engineering for Gas Turbines and Power*, vol. **140**, no. 2, 2018.

Lupo, G. and Duwig, C., Uncertainty quantification of multispecies droplet evaporation models, *International Journal of Heat and Mass Transfer*, vol. **154**, p. 119697, 2020.

Maqua, C., Castanet, G., and Lemoine, F., Bicomponent droplets evaporation: Temperature measurements and modelling, *Fuel*, vol. **87**, no. 13, pp. 2932 – 2942, 2008.

Oberkampf, W.L. and Roy, C.J., *Verification and validation in scientific computing*, Cambridge Univ. Press, Cambridge, 2010.

Prager, J., Najm, H.N., Sargsyan, K., Safta, C., and Pitz, W.J., Uncertainty quantification of reaction mechanisms accounting for correlations introduced by rate rules and fitted arrhenius parameters, *Combustion and flame*, vol. **160**, no. 9, pp. 1583–1593, 2013.

Ra, Y. and Reitz, R.D., A vaporization model for discrete multi-component fuel sprays, *International Journal of Multiphase Flow*, vol. **35**, no. 2, pp. 101–117, 2009.

Rauch, B., Calabria, R., Chiariello, F., Le Clercq, P., Massoli, P., and Rachner, M., Accurate analysis of multicomponent fuel spray evaporation in turbulent flow, *Experiments in Fluids*, vol. **52**, pp. 935–948, 2012.

Rauch, B., Clercq, P.L., and Aigner, M., Application of uncertainty quantification for the validation of spray evaporation models, *27th Annual Conference on Liquid Atomization and Spray Systems (ILASS Europe 2016)*, 2016, DHE-06.

Roy, C.J. and Oberkampf, W.L., A comprehensive framework for verification, validation, and uncertainty quantification in scientific computing, *Computer methods in applied mechanics and engineering*, vol. **200**, no. 25-28, pp. 2131–2144, 2011.

Ruoff, S.J., Rauch, B., Le Clercq, P., and Aigner, M., Assessment of the comparability of droplet evaporation fuel sensitivities between a unit test case and an aviation gas turbine combustor, *AIAA Scitech 2019 Forum*, p. 0727, 2019.

Sanjosé, M., Lederlin, T., Gicquel, L., Cuenot, B., Pitsch, H., Garcia-Rosa, N., Lecourt, R., and Poinsot, T., Les of two-phase reacting flows, *Proceedings of the Summer Program*, Center for Turbulence Research, NASA AMES, Stanford University, USA, pp. 251–264, 2008.

Sazhin, S., Elwardany, A., Sazhina, E., and Heikal, M., A quasi-discrete model for heating and evaporation of complex multicomponent hydrocarbon fuel droplets, *International Journal of Heat and Mass Transfer*, vol. **54**, no. 19-20, pp. 4325–4332, 2011.

Shashank, E.K., Knudsen, E., and Pitsch, H., Spray evaporation model sensitivities, *Annual Research Briefs*, vol. **2011**, pp. 213–224, 2011.

Smolyak, S.A., Quadrature and interpolation formulas for tensor products of certain classes of functions, *Doklady Akademii Nauk*, Vol. 148, Russian Academy of Sciences, pp. 1042–1045, 1963.

Sobol, I.M., Sensitivity estimates for nonlinear mathematical models, *Mathematical modelling and computational experiments*, vol. **1**, no. 4, pp. 407–414, 1993.

Stengele, J., Prommersberger, K., Willmann, M., and Wittig, S., Experimental and theoretical study of one- and two-component droplet vaporization in a high pressure environment, *International Journal of Heat and Mass Transfer*, vol. **42**, no. 14, pp. 2683 – 2694, 1999.

Stöhr, M., Ruoff, S., Rauch, B., Meier, W., and Le Clercq, P., Droplet vaporization for conventional and alternative jet fuels at realistic temperature conditions: Systematic measurements and numerical modeling, *Proceedings of the Combustion Institute*,

2020.

Sudret, B., Global sensitivity analysis using polynomial chaos expansions, *Reliability engineering & system safety*, vol. **93**, no. 7, pp. 964–979, 2008.

Tonini, S. and Cossali, G.E., An analytical approach to model heating and evaporation of multicomponent ellipsoidal drops, *Heat and Mass Transfer*, vol. **55**, no. 5, pp. 1257 – 1269, 2019.

Van Dam, N. and Rutland, C., Uncertainty quantification of large-eddy spray simulations, *Journal of Verification, Validation and Uncertainty Quantification*, vol. **1**, no. 2, 2016.

Verdier, A., Santiago, J.M., Vandel, A., Saengkaew, S., Cabot, G., Grehan, G., and Renou, B., Experimental study of local flame structures and fuel droplet properties of a spray jet flame, *Proceedings of the Combustion Institute*, vol. **36**, no. 2, pp. 2595 – 2602, 2017.

Wilms, J., Evaporation of multicomponent droplets, phdthesis, Fakultät Luft- und Raumfahrttechnik und Geodäsie, Universität Stuttgart, 2005.

Won, S.H., Rock, N., Lim, S.J., Nates, S., Carpenter, D., Emerson, B., Lieuwen, T., Edwards, T., and Dryer, F.L., Preferential vaporization impacts on lean blow-out of liquid fueled combustors, *Combustion and Flame*, vol. **205**, pp. 295–304, 2019.

Xiu, D. and Karniadakis, G.E., Modeling uncertainty in flow simulations via generalized polynomial chaos, *Journal of computational physics*, vol. **187**, no. 1, pp. 137–167, 2003.

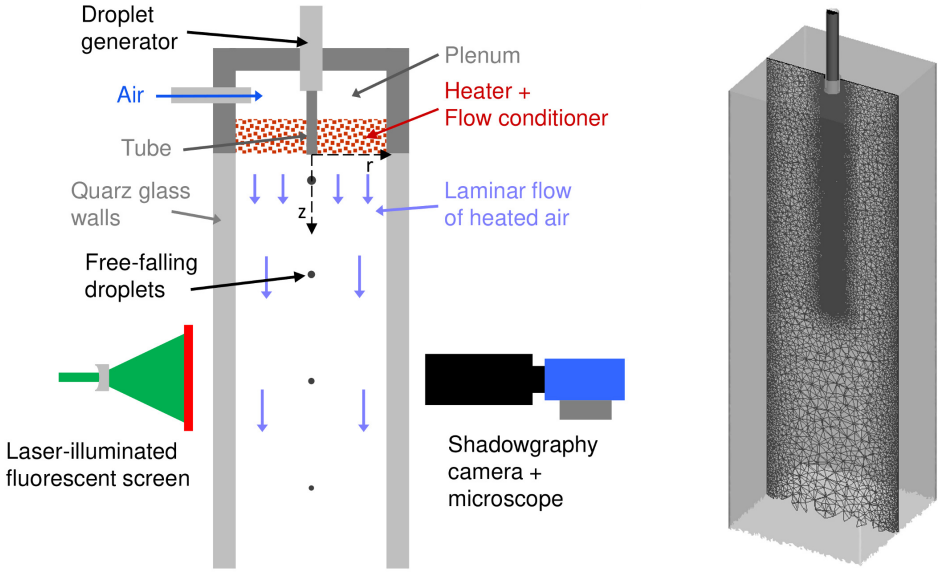

(a) (b)

FIG. 1: Experimental Setup (a) and computational domain and depiction of the grid in a cut plane (b) of the droplet evaporation test case

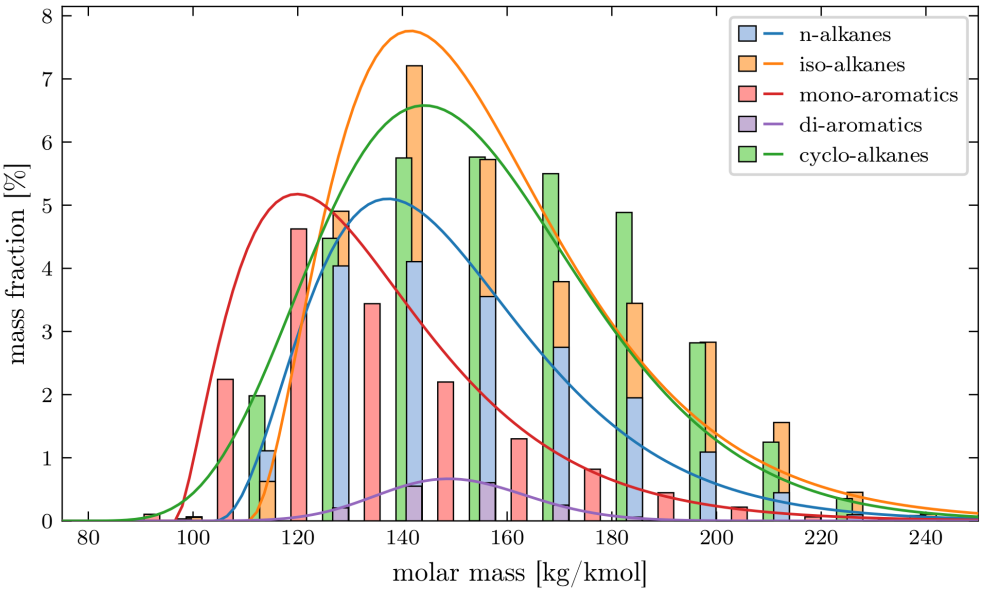

FIG. 2: Fuel composition for a conventional jet fuel clustered by fuel families. Bars indicate the discrete composition, lines the fitted composition by gamma distribution.

TABLE 1: Molar fractions of fuel families of multi-component jet fuels.

Name		n-alkanes	iso-alkanes	mono-aromatics	di-aromatics	cyclo-alkanes
A1	Reference fuel	0.192	0.307	0.155	0.017	0.329
B1	Alcohol-to-Jet	0.000	1.000	0.000	0.000	0.000
C1	High aromatic	0.101	0.150	0.019	0.181	0.549
C5	High volatility	0.110	0.166	0.105	0.118	0.501

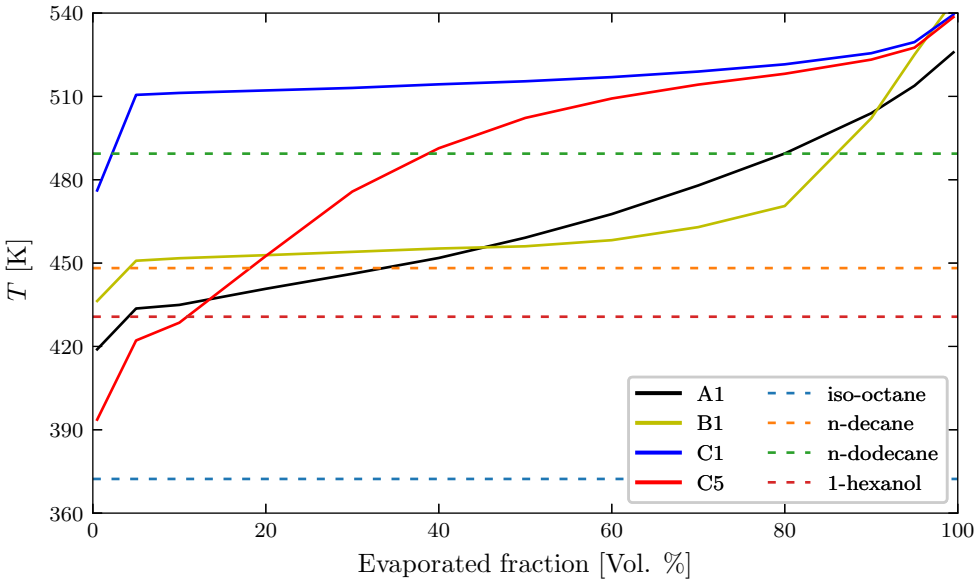

FIG. 3: Distillation curves of multi-component fuels using ASTM International (2004) D86 method (solid lines) and boiling points of single-component fuels(dashed lines) (Kim et al., 2019)

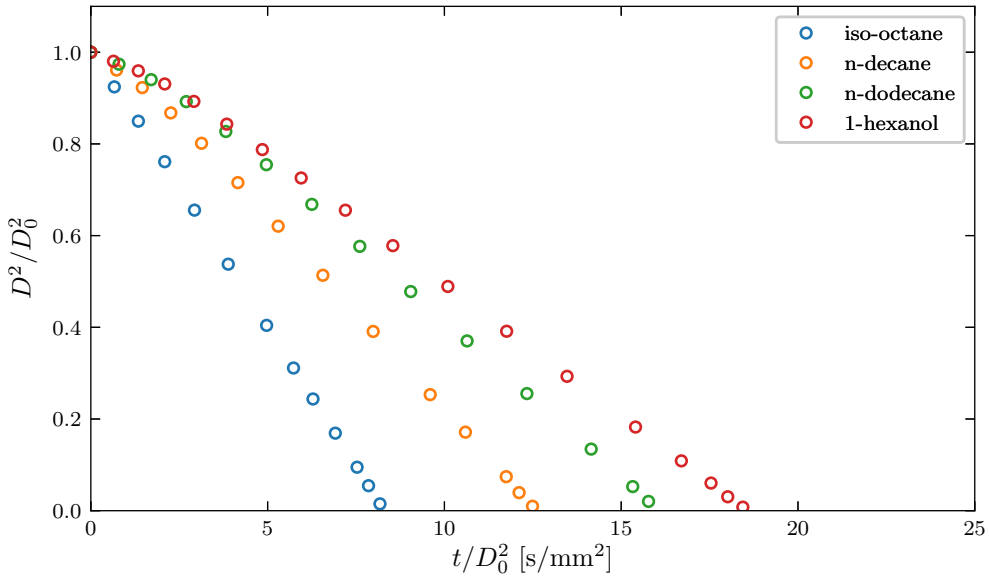

FIG. 4: Experimental results of single component fuels: Temporal evolution of squared droplet diameter D^2, normalized by the squared initial diameter D_0^2. Absolute errors are smaller than 0.01 µm^2/µm^2 and thus not shown.

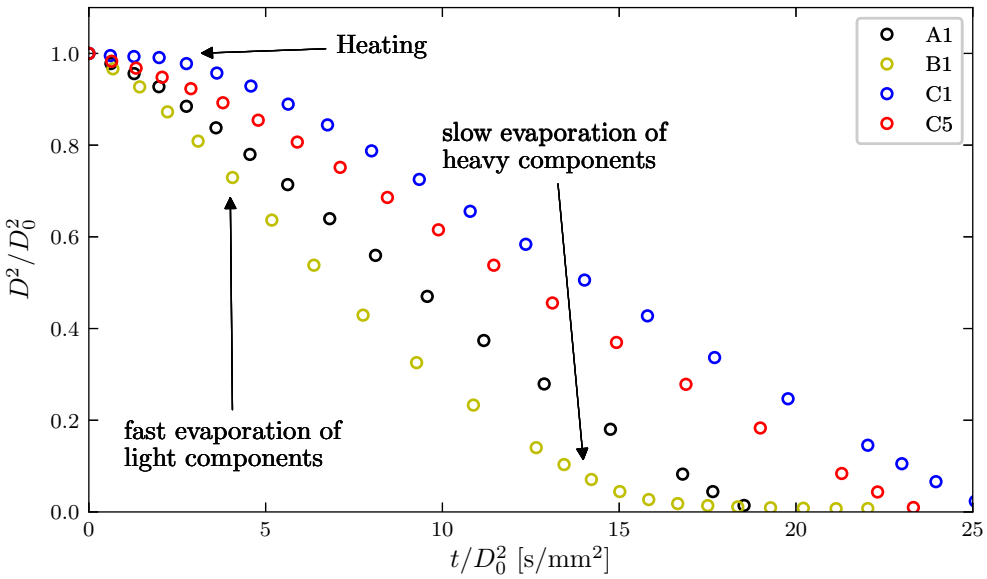

FIG. 5: Experimental results of multi-component fuels: Temporal evolution of squared droplet diameter D^2, normalized by the squared initial diameter D_0^2. Absolute errors are smaller than 0.01 µm^2/µm^2 and thus not shown.

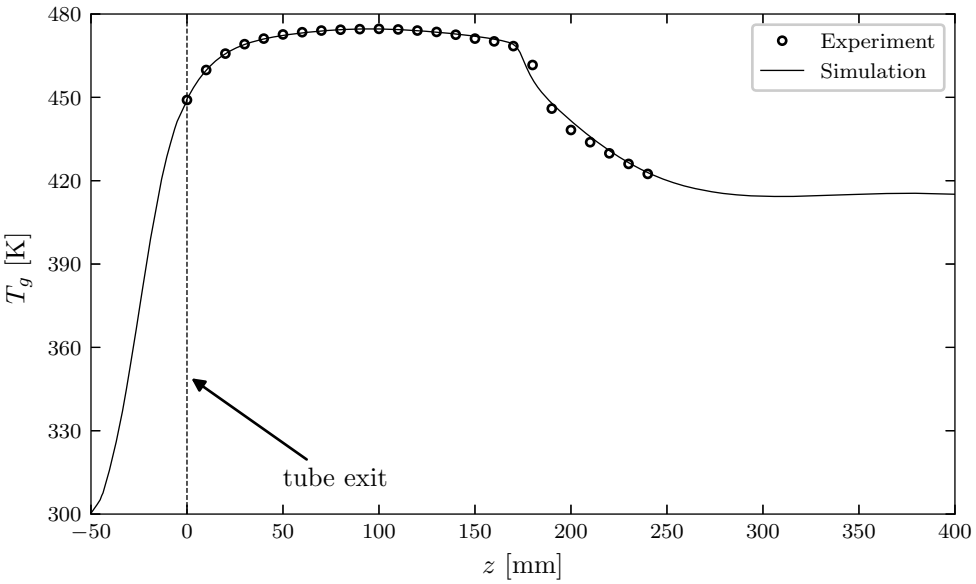

FIG. 6: Centerline profiles of ambient gas temperature $T_g(z)$

TABLE 2: Classification of the boundary conditions by type of method used to determine the values and corresponding uncertainties.

Boundary Condition			Determination method	Value	Uncertainty
Flow	Channel wall temperature at $z = 0\,\mathrm{mm}$	T_0	estimated by num. sim.	460 K	± 15 K
	Channel wall temperature at $z = 100\,\mathrm{mm}$	T_{100}	estimated by num. sim.	305 K	$+15$ K, -10 K
	Channel wall temperature at $z = 200\,\mathrm{mm}$	T_{200}	estimated by num. sim.	300 K	$+15$ K, -5 K
	Matrix Inflow temperature	T_{in}	thermocouple	478 K	± 5 K
	Tube wall temperature	T_{t}	estimated by num. sim.	470 K	± 5 K
Droplets	Droplet initial velocity	v_{d}	manufacturer's specs	$2.0\,\mathrm{m/s}$	$\pm\, 0.2\,\mathrm{m/s}$
	Droplet initial diameter	D_{d}	manufacturer's specs	$80\,\mu\mathrm{m}$	$\pm\, 2\,\mu\mathrm{m}$
	Droplet initial temperature	T_{d}	thermocouple	303.15 K	$\pm$ 1.15 K
	Droplet initial centerline distance	r_{d}	shadowgraphy	$0\,\mathrm{mm}$	$+\, 1.8\,\mathrm{mm}$

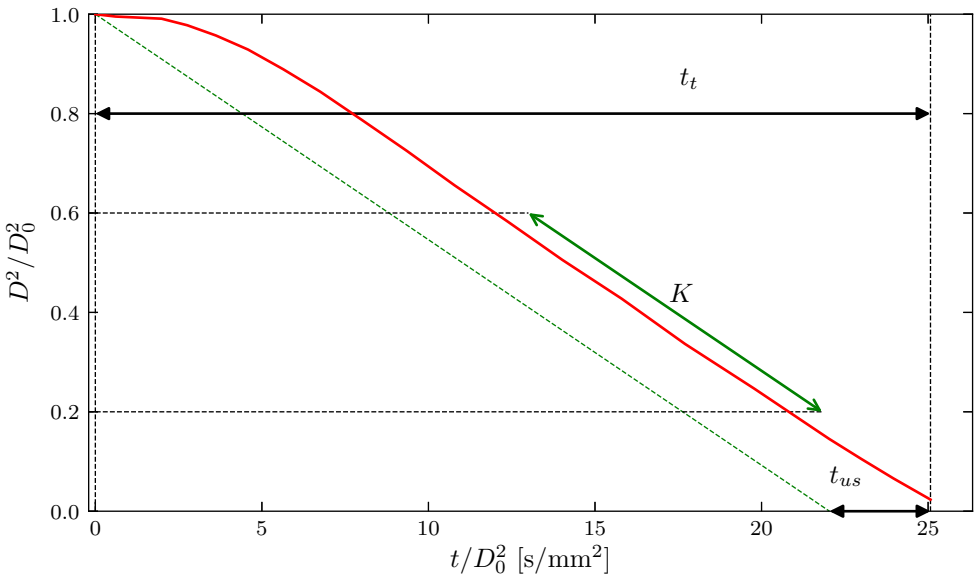

FIG. 7: Evaporation metrics: Total evaporation time t_t, evaporation rate K and unsteady heat-up time t_{us}, adapted from Asrardel et al. (2019)

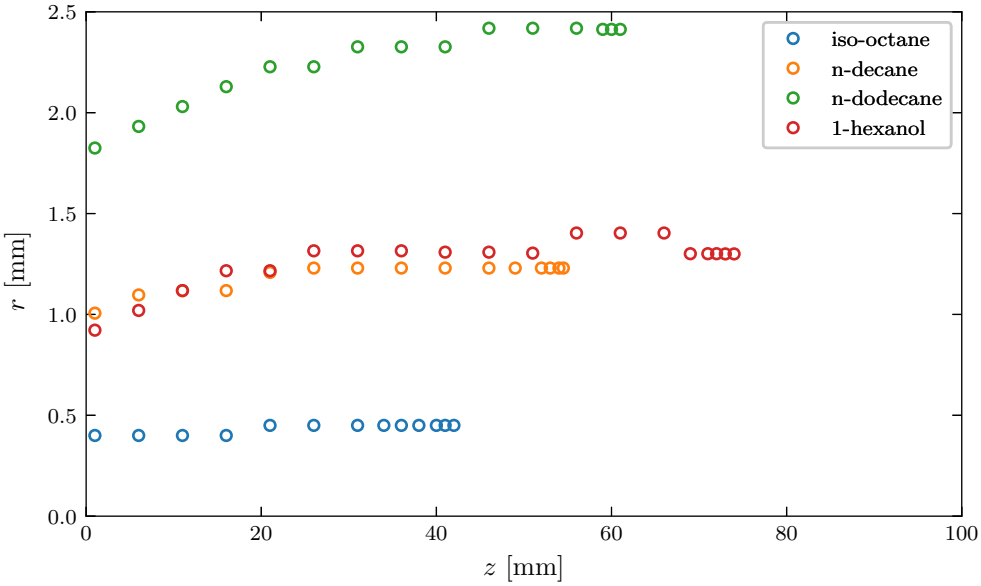

FIG. 8: Experimental results for the radial offset r of the droplets from the centerline ($r = 0\,\mathrm{mm}$)

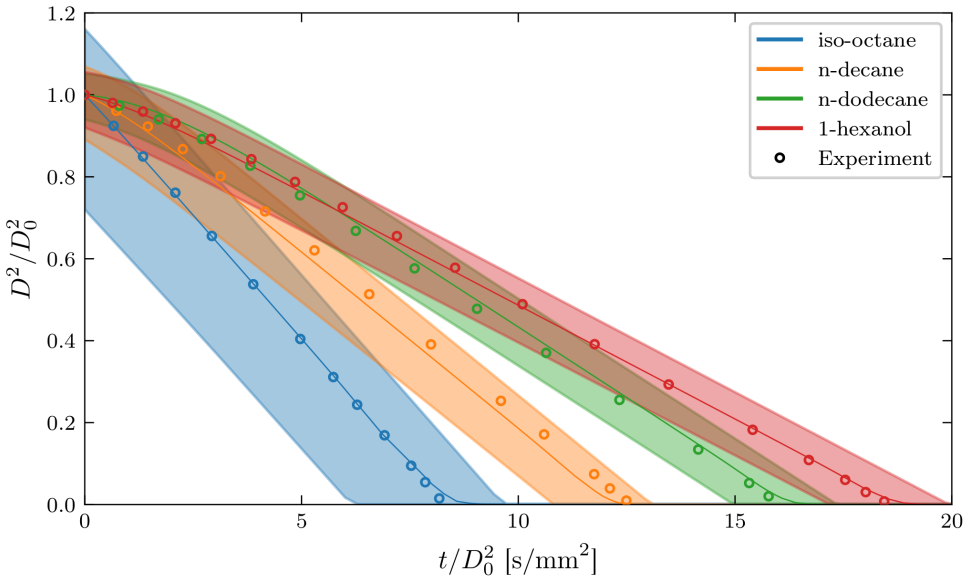

FIG. 9: Comparison of measurements (symbols) and non-deterministic simulations for single component fuels. Solid lines represent the mean $\mathbb{E}$, shaded areas the uncertainties.

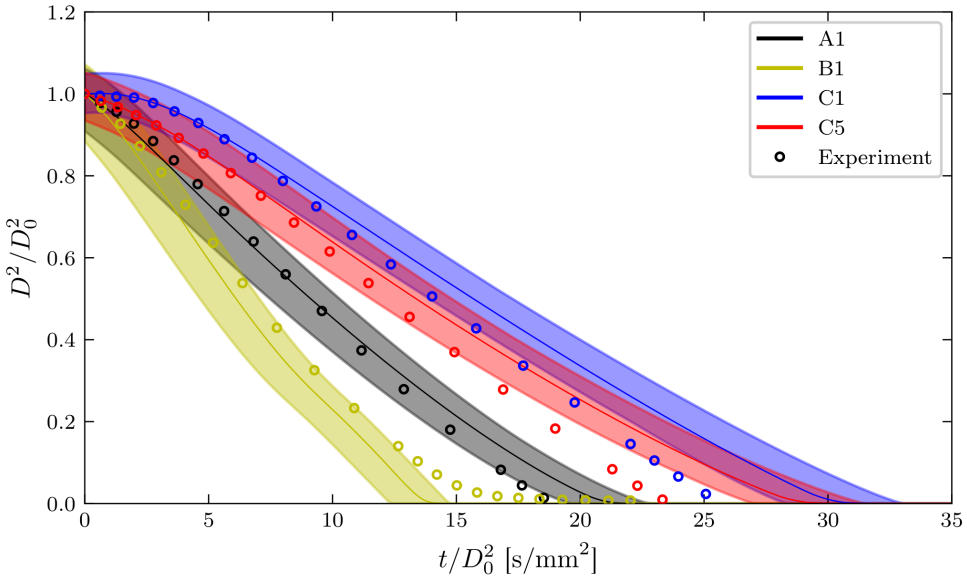

FIG. 10: Comparison of measurements (symbols) and non-deterministic simulations for multi-component fuels. Solid lines represent the mean $\mathbb{E}$, shaded areas the uncertainties.

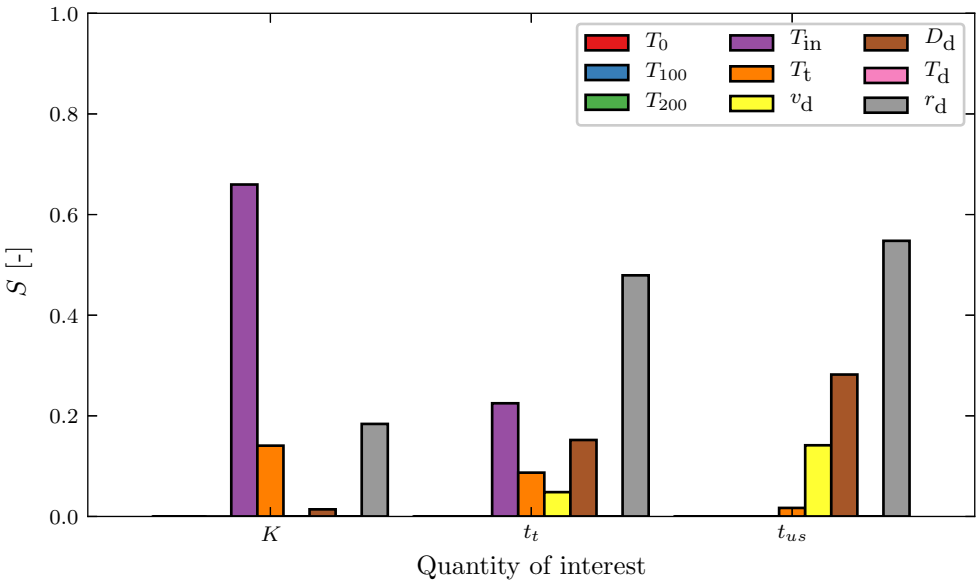

FIG. 11: Main Sobol indices S_i for the evaporation rate K, total evaporation time t_t and unsteady heat-up time t_{us}. The total Sobol indices S_i^T are nearly identical to the main indices and thus not shown.